Evaluating NeRFs for 3D Plant Geometry Reconstruction in Field Conditions

MUHAMMAD ARBAB ARSHAD, Iowa State University, USA

TALUKDER JUBERY, Iowa State University, USA

JAMES AFFUL, Iowa State University, USA

ANUSHRUT JIGNASU, Iowa State University, USA

ADITYA BALU, Iowa State University, USA

BASKAR GANAPATHYSUBRAMANIAN, Iowa State University, USA

SOUMIK SARKAR[*], Iowa State University, USA

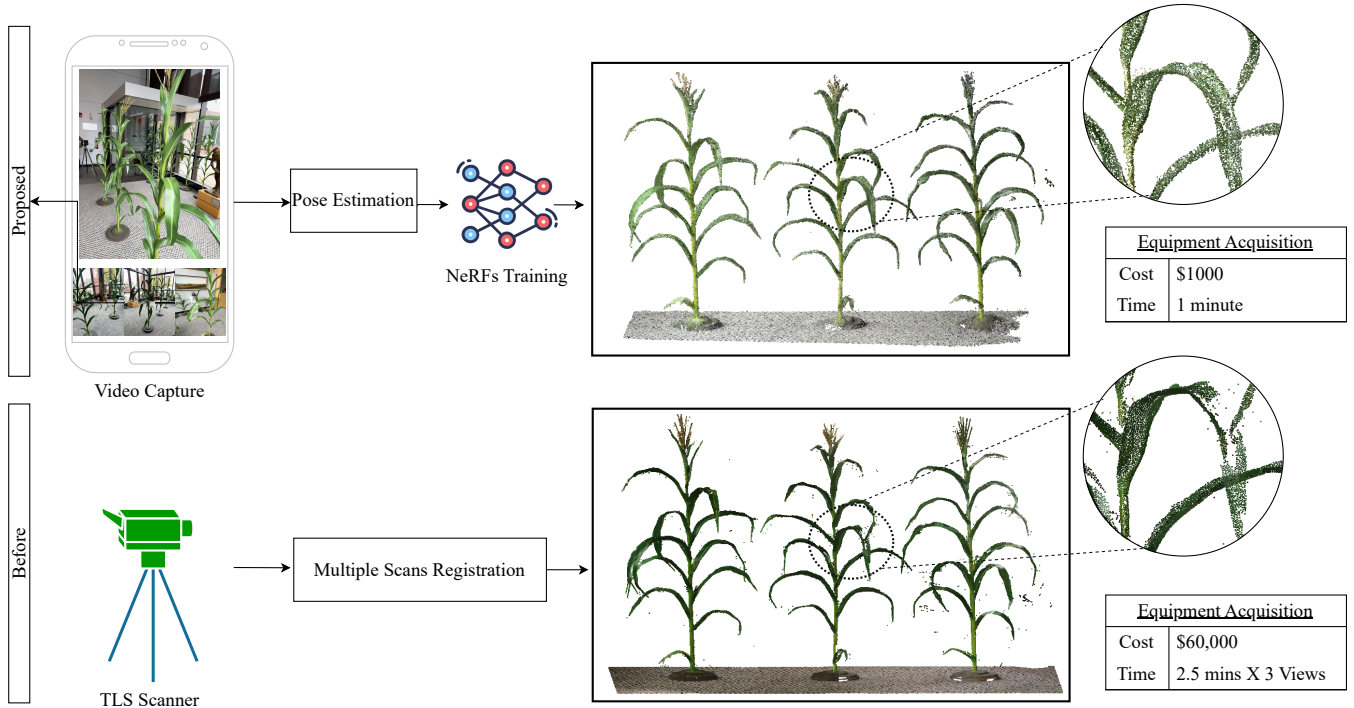ADARSH KRISHNAMURTHY[†], Iowa State University, USA

Fig. 1. *Using NeRFs for 3D reconstruction of plants in field conditions.*

We evaluate different Neural Radiance Fields (NeRFs) techniques for reconstructing (3D) plants in varied environments, from indoor settings to outdoor fields. Traditional techniques often struggle to capture the complex details of plants, which is crucial for botanical and agricultural understanding. We evaluate three scenarios with increasing complexity and compare the results with the point cloud obtained using LiDAR as ground truth data. In the most realistic field scenario, the NeRF models achieve a 74.65% F1 score with 30 minutes of training on the GPU, highlighting the efficiency and accuracy of NeRFs in challenging environments. These findings not only demonstrate the potential of NeRF in detailed and realistic 3D plant modeling but also suggest practical approaches for enhancing the speed and efficiency of the 3D reconstruction process.

[*]Corresponding author.

[†]Corresponding author.

Authors' addresses: Muhammad Arbab Arshad, Iowa State University, USA; Talukder Jubery, Iowa State University, USA; James Afful, Iowa State University, USA; Anushrut Jignasu, Iowa State University, USA; Aditya Balu, Iowa State University, USA; Baskar Ganapathysubramanian, Iowa State University, USA; Soumik Sarkar, soumiks@iastate.edu, Iowa State University, USA; Adarsh Krishnamurthy, adarsh@iastate.edu, Iowa State University, USA.

1 INTRODUCTION

In recent years, the importance of reconstructing 3D geometry has emerged as a critical area within plant sciences. As global challenges in agriculture and botany become increasingly complex [1], gaining a detailed understanding of plant structures has become essential. This goes beyond mere visual representation; capturing the intricate details of plant morphology provides valuable insights into their growth, responses to environmental stressors, and physiological processes [2, 3]. NeRF emerges as a pivotal innovation in the domain of 3D geometry reconstruction.

At its core, NeRF (Neural Radiance Fields) represents a ground-breaking technique that utilizes the capabilities of deep learning to synthesize continuous 3D scenes by modeling the volumetric scene function [4]. This approach significantly advances beyond traditional methods such as structure from motion (SfM) [5] and Multi View Stereo (MVS) [6], which rely on the analysis of discrete 2D pixels, thus marking a new era in the field of 3D model reconstruction.Unlike its predecessors, NeRF enables the rendering of photorealistic scenes from any viewpoint using a set of 2D images, without necessitating explicit 3D geometry or depth maps. This is primarily due to NeRF's use of implicit representation models, in contrast to the explicit representations like point clouds in Structure from Motion (SfM) and voxel grids in Multi View Stereo (MVS), which inherently limit the quality of the reconstruction. The implicit representation utilized by NeRF is resolution invariant, allowing for significantly more detailed and granular modeling without the constraints of resolution-dependent methods. This innovation not only enhances the reconstruction of complex scenes but also holds the promise of revolutionizing the 3D modeling of plant structures by providing an unprecedented level of detail and granularity. The versatility and rapid adoption of NeRF as a state-of-the-art technique underscore its significance, with applications ranging from virtual reality [7] to architectural reconstructions [8]. Particularly in botany and plant research, NeRF's ability to capture the finest details offers potential for groundbreaking insights into plant structures, establishing it as a key tool in the advancement of modern botanical studies. However, translating this potential into practical applications presents its own set of obstacles.

1.1 Challenges in 3D Plant Modeling

Contemporary 3D modeling techniques for plant structures face significant challenges when attempting to capture the minute details inherent in plants [2]. The complexity of plants, from their delicate leaf venation [9] to intricate branching patterns [10], necessitates models that encompass these specific details. A summary of these is given in Table 1

1.1.1 Technical Challenges. Traditional methodologies like photogrammetry are adept at large-scale reconstructions, but often overlook these subtle intricacies [11–13]. Utilizing tools such as FARO 3D LiDAR scanners have been adopted for 3D reconstructions of plants like maize [12] and tomatoes [13]. However, to capture every detail, data from multiple angles is essential. This poses a challenge since scanning from each side using devices like FARO 3D LiDAR scanners is time-consuming, limiting the number of angles that can be efficiently captured. Due to the limited poses, this approach does not scale well to capture minute details in large scenes, and consequently, some desired details might be missed in the final model. Andújar et al. have emphasized that, even with advanced sensors, there are gaps in detailed reconstruction and the preservation of essential information for intricate applications [14]. They also point out that while devices such as the MultiSense S7 from Carnegie Robotics combine lasers, depth cameras, and stereo vision to offer commendable results, the high acquisition costs can be prohibitive. The complexity extends beyond static to dynamic realms.

In addition to the aforementioned challenges, the dynamic nature of flexible objects like plants and environmental dynamism introduce an added dimension of complexity. Plants, unlike static entities, undergo growth, exhibit movement in reaction to environmental stimuli, and demonstrate both diurnal and seasonal variations. The environmental dynamism, coupled with plant behavior, further complicates modeling efforts. Paturkar et al.'s comprehensive investigation underscores that this dynamism inherently complicates the attainment of precise 3D models. Factors such as persistent growth, environmental dynamism, and external perturbations, notably in windy scenarios, jeopardize the consistency of data acquisition during imaging processes [11, 15, 16]. This complexity necessitates innovative solutions in 3D modeling and data processing.

Furthermore, an array of 3D modeling approaches mandate rigorous [17], an exercise that necessitates vast computational capacities and specialized knowledge. This post-processing phase, being resource and time-intensive, often becomes a constraining factor in projects, particularly when modifications or refinements are imperative based on novel data or feedback. As emphasized in Liénard et al. [18], discrepancies during the post-processing phase in UAV imagery-centric 3D scene reconstruction might culminate in costly and irreversible repercussions. This necessitates a reevaluation of the cost-benefit ratio inherent in these technologies.

1.1.2 Accessibility Challenges. These factors indicate that the challenges in capturing every facet of plant structures remain, even when employing sophisticated sensors. Financial implications further exacerbate these challenges. Although techniques like terrasential LiDAR scanners provide superior accuracy, their exorbitant costs often render them inaccessible to a significant portion of researchers. Tang et al. delineate that the substantial financial commitment associated with such advanced equipment, combined with the specialized expertise requisite for its operation, significantly limits their adoption within both academic and enthusiast domains [19]. Recognizing these barriers, our study proposes an innovative solution.

1.2 Objectives and Significance of the Study

This study focuses on a detailed evaluation of advanced Neural Radiance Fields (NeRF) methodologies to assess their applicability and effectiveness in high-resolution 3D modeling of plant structures. Traditional 3D modeling techniques often fall short when

Table 1. *Challenges in 3D Modeling Techniques for Plant Structures*

Technical Challenges	Accessibility Challenges
Detail limitations in Photogrammetry	High acquisition costs
Data acquisition from multiple angles	Limited equipment accessibility
Dynamic nature of plants	Expertise for operation
Environmental dynamism	
Rigorous post-processing	

it comes to accurately capturing the complex and dynamic morphology of plants [20]. Our research aims to explore how NeRF can address these limitations, offering a more nuanced and detailed approach to modeling plant structures. Bridging this gap, our study integrates cutting-edge NeRF techniques with mobile technology advancements.

A pivotal aspect of our methodology is the use of mobile technology for data acquisition. By utilizing the widespread availability and sophisticated capabilities of modern smartphones, we aim to make high-quality 3D data collection more accessible and cost-effective. This approach, combined with the NeRF framework's ability to process a wide variety of image datasets, is expected to revolutionize 3D plant modeling practices, enhancing both inclusivity and efficiency. Next, we delve into the specifics of our research.

An essential part of our study involves a comparative analysis of different NeRF implementations to determine the most effective configurations for specific modeling needs. This includes assessing detail fidelity, computational efficiency, and the ability to adapt to changes in environmental conditions. Such comparative analysis is crucial for establishing benchmarks for NeRF's current capabilities and for identifying opportunities for future technological improvements. We summarize our contributions as follows:

(1) A dataset collection encompassing a wide range of plant scenarios for reconstruction purposes consisting of images, camera poses, and ground truth TLS scans.

(2) An evaluation of state-of-the-art NeRF techniques across seven different metrics, offering insights for further research.

(3) The development of an end-to-end evaluation framework designed to reassess future reconstruction technologies, specifically for 3D modeling in plant sciences.

Furthermore, a comprehensive review of related works and NeRF techniques mentioned in the literature is provided in Table 2, setting the stage for our investigation.

2 MATERIALS AND METHODS

2.1 Field scenarios

In order to evaluate the efficacy of NeRF techniques across varying complexities and conditions, three scenarios are considered:

(1) **Single Corn Plant Indoor:** This serves as the simplest test case. A solitary corn plant is placed in a controlled indoor environment. The lighting, background, and other environmental factors are kept constant. The objective is to assess the basic capabilities of NeRF in reconstructing an individual plant structure [26].

(2) **Multiple Corn Plants Indoor:** In this case, more than one corn plant is situated in an indoor setting. The increased complexity due to multiple plants poses a greater challenge for the 3D reconstruction. Inter-plant occlusions and varying plant orientations add an additional layer of complexity.

(3) **Multiple Corn Plants in a Field with Other Plants:** This scenario represents a real-world agricultural field, where corn plants are interspersed with other types of plants. The added complexity due to variable lighting, wind, and other dynamic environmental conditions tests the robustness of the NeRF technology.

2.2 Data Collection

In this experiment, our focus is exclusively on corn plants. We examine three distinct scenarios, elaborated subsequently, spanning from controlled indoor settings to dynamic outdoor ones. In the first scenario, we place a single corn plant in an indoor setting. In the second scenario, we place three corn plants side by side in indoor settings. In the third scenario, in the dynamic outdoor conditions of an experimental field at Iowa State University, we selected a row plot of corn plants planted at approximately 0.2 m distance, approximately at the V12 stage. The leaves between two neighboring plants are overlapping. Transitioning from the specific experimental setups, we now detail the data collection methods utilized in these scenarios.

Our training dataset for NeRF is sourced from RGB images and LiDAR data captured using a mobile phone, with the RGB images aiding in the 3D reconstruction of the plants and the LiDAR exclusively for pose capture. For all three scenarios, data is captured using an iPhone 13 Pro featuring 4K resolution. The device is held at a constant height while circling the plant to ensure consistent capture angles. The data collection process utilizes the Polycam app, with a time of approximately 2.5 minutes for scenario 3 (multiple plants in the outdoor setting) and around 1 minute for scenario 1 (single plant in the indoor setting). To establish accurate ground truth, we utilized high-definition terrestrial LiDAR scans using the Faro® Focus S350 Scanner. The scanner boasts an angular resolution of 0.011 degrees, equating to a 1.5 mm point spacing over a 10 m scanning range. With the capacity to acquire point clouds of up to 700 million points (MP) at 1 million points per second. Additionally, the scanner includes a built-in RGB camera that captures 360-degree images once the scanning process is complete.

Table 2. *Techniques in Literature.*
†*Used original paper implementation.*
‡*Used implementation from Framework (NeRFStudio/SDFStudio).*

Instant-NGP	NeRFacto	Mip-NeRF	NeRFs	Additional Techniques
Towards a Robust Framework for NeRF Evaluation[21]				
✓‡	✓‡	✓‡	✗	✗
Analyzing the Internals of Neural Radiance Fields[22]				
✗	✓‡	✓‡	✓‡	✗
SteerNeRF: Accelerating NeRF Rendering via Smooth Viewpoint Trajectory[23]				
✓‡	✗	✗	✓†	NSVF, KiloNeRF, PlenOctree, DIVeR
A Critical Analysis of NeRF-Based 3D Reconstruction[24]				
✓†	✓‡	✗	✗	Tensorf, Mono-Neus, Neus-Facto, MonoSDF, VolSDF, NeuS, UniSurf
Few-Shot Photogrametry: NeRF vs. MVS-SfM in Cultural Heritage Documentation[25]				
✓†	✗	✗	✗	✗

Both in indoor and outdoor settings, we scan the plants from four (for the single plant) to six (for multiple plants) locations around the plant(s), at a height of 1.5 m and a distance of 1.5 m from the plant(s). To reduce the movement of the leaves during scanning, in indoor settings, we ensure that there is no airflow around the plants, and in outdoor settings, we waited for a suitable time when there was negligible wind flow (August 31, 2023, at 8:30 a.m.). Each scan required approximately 2 minutes and 24 seconds, totaling a capture time of around 18 minutes in outdoor settings, including manually moving the scanner around the plot. The six scans were processed in SCENE® software to add RGB color data to the point clouds, followed by the registration of the clouds by minimizing cloud-to-cloud distance and top view distance. Afterward, we cropped out the area of interest from the registered point cloud, removed duplicate points, and reduced noise using statistical outlier removal based on global and local point-to-point distance distributions. This process resulted in the point cloud having an average resolution of about 7 mm.

This experimental setup enables the NeRF algorithm to work on a range of complexities, from controlled environments to dynamic, real-world conditions.

2.3 Camera Pose, NeRF Training, and Pointcloud Exports

Camera pose estimation is a crucial second step, typically achieved through a Structure from Motion (SfM) pipeline such as colmap. This process is essential for obtaining accurate 3D structures from sequences of images by determining correspondences between feature points and by using sequential matching, especially effective since our dataset comprises video frames.

In our workflow, we incorporate cutting-edge NeRF models for their rapid prototyping capabilities, which are critical in plant sciences to enable large scale reconstructions. Specifically, we employ Instant-NGP [27], Nerfacto [28], and TensoRF [29], trained on an Nvidia A100 GPU with 80GB of memory. These models are at the forefront of efficiency, with vanilla NeRF requiring approximately 50 times longer to achieve comparable results. Notably, Instant-NGP introduces a small neural network complemented by a multiresolution

hash table, optimizing the number of operations required for training and rendering [27]. TensoRF, on the other hand, conceptualizes the radiance field as a 4D tensor and applies tensor decomposition to achieve better rendering quality and faster reconstruction times compared to the traditional NeRF approach [29].

Nerfacto synthesizes various techniques from multiple contributions in the field, such as the Multilayer Perceptron (MLP) adapted from Instant-NGP, and the Proposal Network Sampler from MipNeRF-360 [30], as depicted in the attached image. Post-training, the models are converted into pointclouds with a million points each. The effectiveness of these reconstructions is then rigorously assessed as outlined in the next section.

2.4 Evaluation

2.4.1 Pipline. We reconstruct the scene and capture point clouds using a FARO scan for ground truth. To perform a one-to-one comparison between the NeRF-based reconstruction and ground truth, alignment is crucial. Our alignment and evaluation methodology is adapted from Knapitsch et al. [31]. In their work, they evaluate different pipelines and use colmmap as a 'arbitrary reference' frame. However, in our case, all the NeRFs use colmap in their pipeline so the reference frame and reconstruction frame becomes the same. This simplifies the steps and the updated steps, used in our paper are given below:

(1) **Preliminary Camera Trajectory Alignment**: The NeRF-reconstructed point cloud is manually aligned with the ground truth using point-based alignment. Four corresponding points are selected in both point clouds to compute an initial transformation matrix. This matrix aligns the camera poses, providing initial scale and orientation estimates. This initial Coarse-grained alignment step paves the way for more detailed alignment procedures.

(2) **Cropping**: Each ground-truth model has a manually-defined bounding volume, outlining the evaluation region for reconstructions.
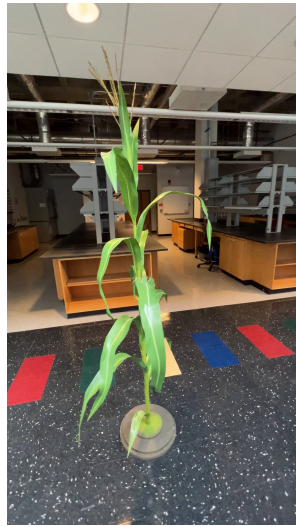
(a) *Frame 1* (b) *Frame 2* (c) *Frame 3* (d) *Frame 4*

Fig. 2. *Raw Images Provided to NeRFs - Scenario I*

(a) *Frame 1* (b) *Frame 2* (c) *Frame 3* (d) *Frame 4*

Fig. 3. *Raw Images Provided to NeRFs - Scenario II*

(a) *Frame 1* (b) *Frame 2* (c) *Frame 3* (d) *Frame 4*

Fig. 4. *Raw Images Provided to NeRFs - Scenario III*

(3) **ICP Registration**: Drawing inspiration from the iterative refinement process detailed by Besl et al. [32] and further refined by Zhang et al. [33], we adopt a three-stage approach as introduced by Knapitsch et al. [31] for our initial registration framework. The process begins with a specified voxel size and an associated threshold for the initial registration. In the next iteration, the transformation result from the previous step is used as a starting point, with the voxel size reduced by half to achieve finer detail in the registration. The third stage aims to refine the alignment further by returning to the original voxel size and adjusting the threshold to facilitate convergence at each stage. This multi-scale strategy is designed to capture both coarse and fine details, thereby improving the accuracy and precision of the model alignment. However, in our adaptation for plant structure reconstruction, we diverged from Knapitsch et al. by maintaining the iterative process within a single stage rather than expanding across multiple stages. We found that increasing the iteration count tenfold, rather than the number of stages, prevented the registration process from collapsing [34].

2.4.2 Metrics. To assess the similarity between the ground truth (obtained from TLS) and the reconstructed 3D pointcloud, the following metrics are employed:

(1) **Precision/Accuracy.** Given a reconstructed point set $\mathcal{R}$ and a ground truth set $\mathcal{G}$, the precision metric $P(d)$ assesses the proximity of points in $\mathcal{R}$ to $\mathcal{G}$ within a distance threshold d. Mathematically, it is formulated as:

$$P(d) = \frac{100}{|\mathcal{R}|} \sum_{\mathbf{r} \in \mathcal{R}} \mathbb{I}\left(\min_{\mathbf{g} \in \mathcal{G}} \|\mathbf{r} - \mathbf{g}\| < d\right),$$

where $\mathbb{I}(\cdot)$ is an indicator function.

(2) **Recall/Completeness.** Conversely, the recall metric $R(d)$ quantifies how well the reconstruction $\mathcal{R}$ encompasses the points in the ground truth $\mathcal{G}$ for a given distance threshold d. It is defined as:

$$R(d) = \frac{100}{|\mathcal{G}|} \sum_{\mathbf{g} \in \mathcal{G}} \mathbb{I}\left(\min_{\mathbf{r} \in \mathcal{R}} \|\mathbf{g} - \mathbf{r}\| < d\right).$$

Both the above two metrics are extensively utilized in recent studies. [25, 35].

(3) **F-score.** The F-score, denoted as $F(d)$, serves as a harmonic summary measure that encapsulates both the precision $P(d)$ and recall $R(d)$ for a given distance threshold d. It is specifically designed to penalize extreme imbalances between $P(d)$ and $R(d)$. Mathematically, it can be expressed as:

$$F(d) = \frac{2 \times P(d) \times R(d)}{P(d) + R(d)}.$$

The harmonic nature of the F-score ensures that if either $P(d)$ or $R(d)$ approaches zero, the F-score will also tend towards zero, providing a more robust summary statistic than the arithmetic mean. The value of d was considered 0.005 for first two scenarios and 0.01 for the last scenario.

(4) Traditional metrics such as, **SSIM** [36], **PSNR** [37], **LPIPS** [38] are used to evaluate the quality of the rendered images. These metrics do not need the 3D ground truth and are widely used in literature [39, 40] for evaluation.

2.4.3 Visualization Color Interpretation. The color-coded visualizations employed in our research provide an intuitive understanding of spatial relationships within the 3D reconstructed plant structures. The color gradients signify varying distances from a specific reference point, enabling a comprehensive assessment of depth and intricacy. Specifically:

(1) **Grey**: Represents regions of the plant structure that are closer or have the least distance to a particular reference.

(2) **Red**: Depicts intermediate distances of points from the reference pointcloud within the plant structure.

(3) **Black**: Highlights the furthest points or regions within the reconstructed structure.

3 RESULTS

The results from all the scenarios are provided below:

3.1 Scenario I - Single Plants Indoors

The estimated camera poses from colmap are visualized in Fig. 6. The results from our evaluation of three state-of-the-art NeRF techniques for 3D plant structure reconstruction are illustrated in the Fig. 7.

Precision: Across all models, precision generally increases with the number of iterations. Instant-NGP shows a significant leap in precision from 100 to 5000 iterations (0.29 to 21.93), indicating a drastic improvement in the accuracy of reconstructed points relative to the ground truth. NeRFacto demonstrates a more consistent and steep rise in precision, reaching a peak of 73.57 at 30000 iterations, which surpasses Instant-NGP's best precision. TensoRF, however, shows a relatively modest increase in precision, suggesting its limited capability in accurately capturing fine details compared to the other two models. It is further illustrated in Fig. 8.

Recall: The recall metric follows a similar trend, with Instant-NGP and NeRFacto showing substantial increases with more iterations, indicating an enhanced ability to encompass points from the ground truth. Notably, NeRFacto achieves remarkably high recall values (over 90) at higher iterations (10000 and above), suggesting its superiority in completeness of reconstruction. TensoRF's recall values are significantly lower, suggesting that it may miss more details from the ground truth compared to the other models. It is further illustrated in Fig. 9.

F1 Score: The F1 score, balancing precision and recall, highlights NeRFacto as the most balanced model, especially at higher iterations, with scores above 80. Instant-NGP shows a significant improvement in F1 scores as iterations increase, but it doesn't reach the heights of NeRFacto. TensoRF lags behind in this metric, indicating a less balanced performance between precision and recall.

PSNR:. The Peak Signal-to-Noise Ratio (PSNR) reflects the quality of rendered images. In this metric, Instant-NGP and NeRFacto show
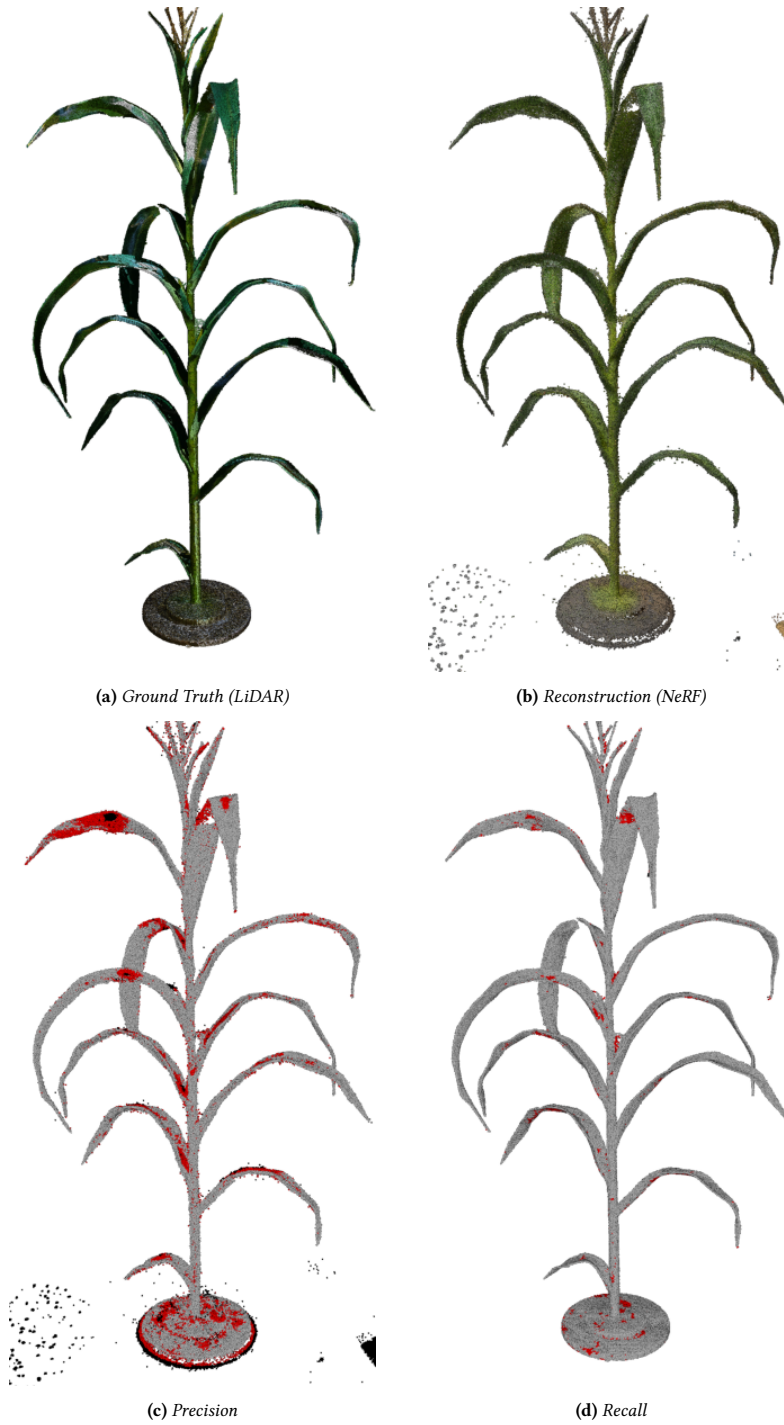
(a) *Ground Truth (LiDAR)*

(b) *Reconstruction (NeRF)*

(c) *Precision*

(d) *Recall*

Fig. 5. *Visualization for Metrics*

a gradual increase in PSNR with more iterations, suggesting improved image quality. TensoRF's PSNR values are lower, indicating potentially lower image quality throughout its iterations.

SSIM:. The Structural Similarity Index (SSIM) is another measure of image quality, assessing the perceived change in structural information. Here, NeRFacto and Instant-NGP both show a steady increase in SSIM with more iterations, with NeRFacto achieving

Fig. 6. *Camera Pose Estimations for Scenario-I*

(a) *PSNR* **(b)** *SSIM* **(c)** *LPIPS*

(d) *Precision* **(e)** *Recall* **(f)** *F1 Score*

Number of Iterations
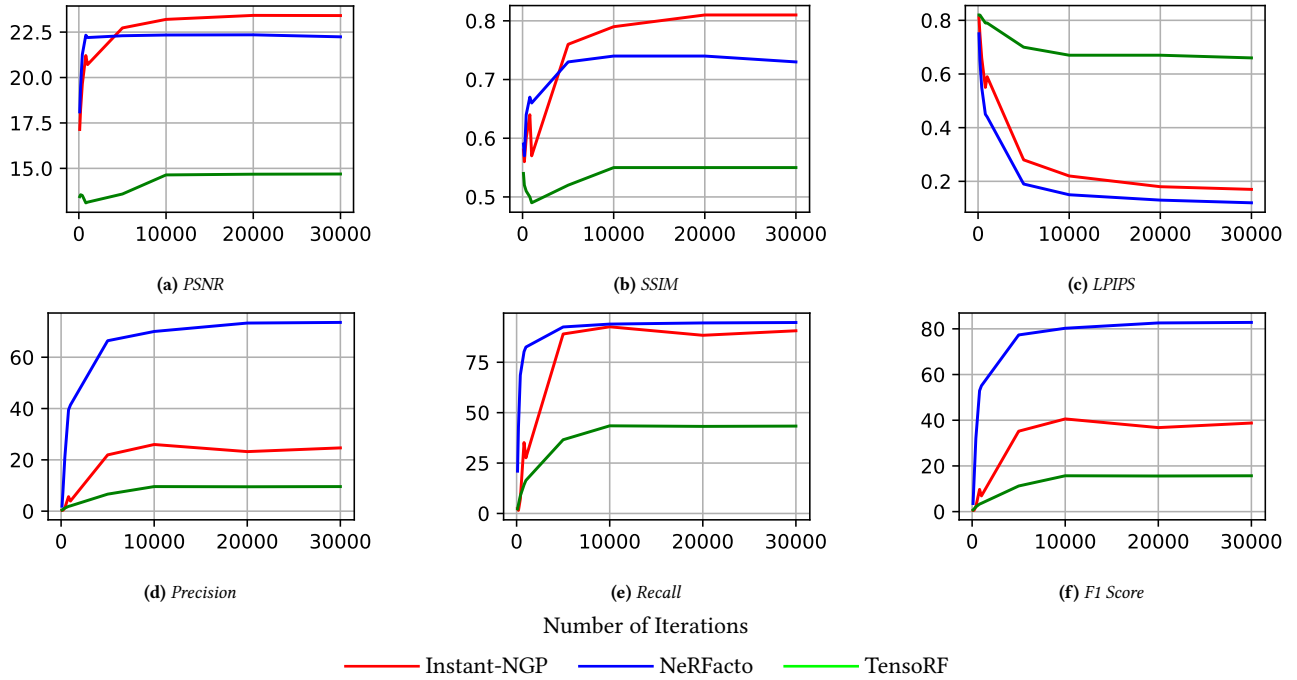
—— Instant-NGP —— NeRFacto —— TensoRF

Fig. 7. *Combined Comparison of 2D Image Quality (top) and 3D Geometry (bottom) Metrics for Scenario-I*

slightly higher scores, suggesting better preservation of structural information in its renderings. TensoRF, again, shows relatively lower SSIM scores.

LPIPS:. The Lower Perceptual Image Patch Similarity (LPIPS) metric indicates perceived image similarity, with lower values being better. NeRFacto and Instant-NGP both show a significant decrease in LPIPS with more iterations, indicating improved perceptual similarity to the ground truth. TensoRF's LPIPS values are consistently higher, suggesting lower perceptual similarity.

Computation Time: Time efficiency is a crucial factor, especially for practical applications. Instant-NGP demonstrates a relatively balanced approach between efficiency and performance, with time increments correlating reasonably with the increase in iterations. However, it becomes significantly time-consuming at very high iterations (20000 and 30000). NeRFacto, while showing superior performance in many metrics, demands considerably more time, especially at higher iterations, which could be a limiting factor in time-sensitive scenarios. TensoRF, despite its lower performance in
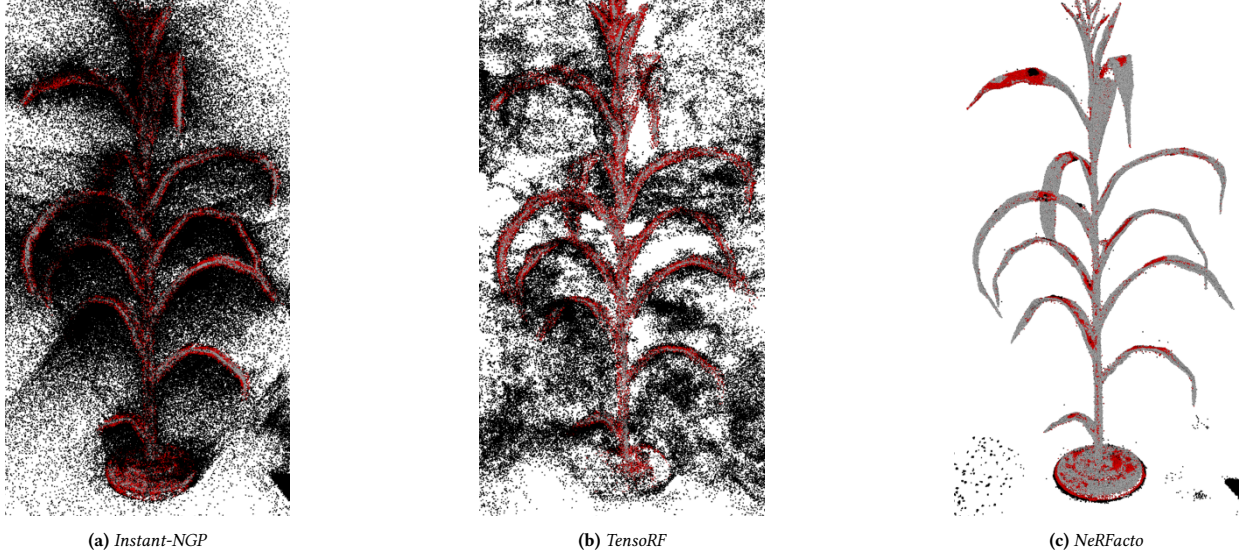
(a) *Instant-NGP*　　　　　　(b) *TensoRF*　　　　　　(c) *NeRFacto*

Fig. 8. *Precision of 3D reconstruction of NeRF techniques*

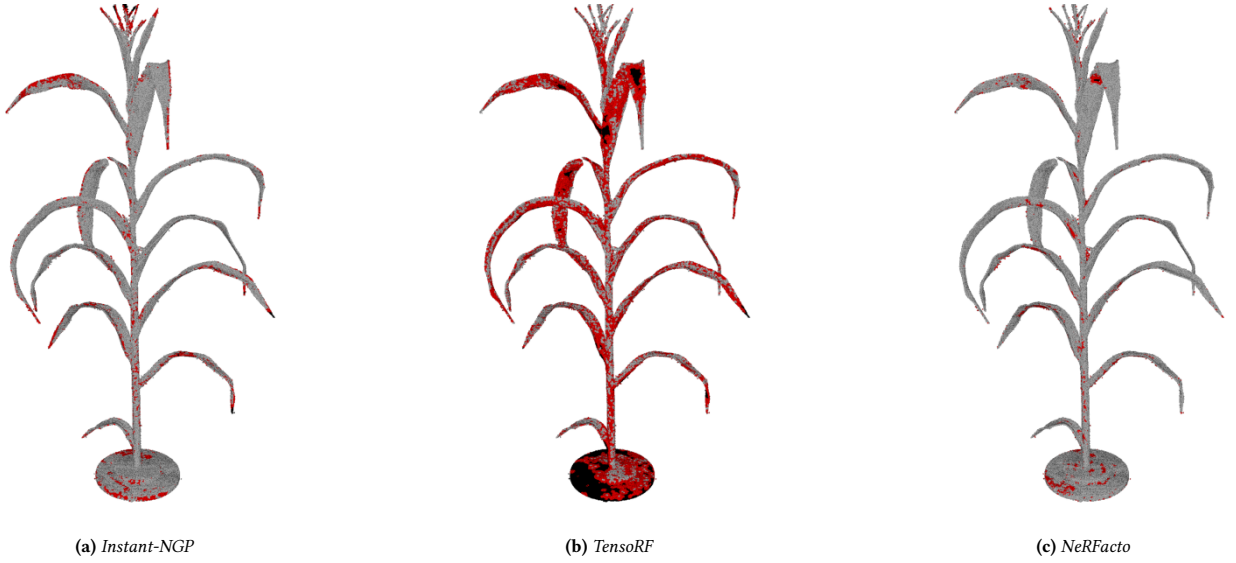(a) *Instant-NGP*　　　　　　(b) *TensoRF*　　　　　　(c) *NeRFacto*

Fig. 9. *Recall of 3D reconstruction of NeRF techniques*

other metrics, maintains a more consistent time efficiency, suggesting its suitability for applications where time is a critical constraint. For the best performing model, it is further illustrated in Fig. 10

Overall Performance and Suitability: In sum, NeRFacto emerges as the most robust model in terms of precision, recall, F1 score, and image quality metrics (PSNR, SSIM, LPIPS), making it highly suitable for applications demanding high accuracy and completeness in 3D modeling. However, its time inefficiency at higher iterations might restrict its use in time-sensitive contexts. Instant-NGP presents a good balance between performance and efficiency, making it a viable option for moderately demanding scenarios. Detailed results are given in Table 3, after complete training. For more granular look,

consult the supplementary Table 6. The Precision-Recall Curves based on varying distance threshold after maximum training of 30,000 iterations is given in Fig. 11

Insight 1: Computational Cost and Accuracy Trade-off in Instant-NGP and NeRFacto: The steep increase in performance metrics with the number of iterations for both Instant-NGP and NeRFacto suggests that these models require a substantial amount of data processing to achieve high accuracy, which is critical in high-fidelity 3D modeling. However, this also implies a higher computational cost, which needs to be considered in practical applications.
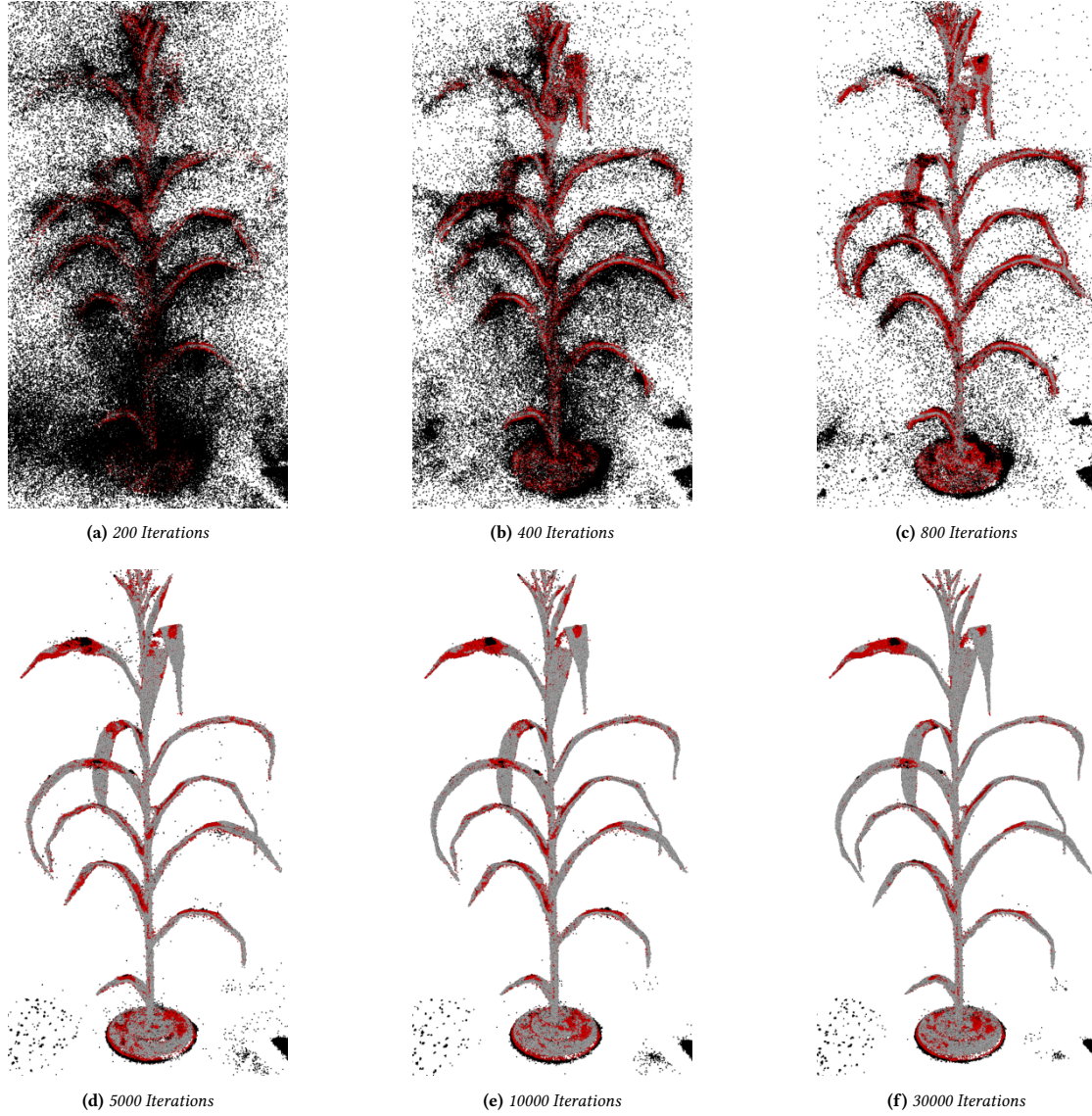
(a) *200 Iterations* **(b)** *400 Iterations* **(c)** *800 Iterations*

(d) *5000 Iterations* **(e)** *10000 Iterations* **(f)** *30000 Iterations*

Fig. 10. *Precision Over Training Iterations for NeRFacto - Scenario 1*

Table 3. *Performance metrics of NeRFs reconstruction techniques - Scenario I*

Model Name	Precision ↑	Recall ↑	F1 ↑	PSNR ↑	SSIM ↑	LPIPS ↓	Time(s) ↓
Instant-NGP	24.66	90.62	38.77	23.41	0.81	0.17	756
NeRFacto	73.57	94.72	82.81	22.24	0.73	0.12	1938
TensoRF	9.58	43.34	15.69	14.69	0.55	0.66	1973

Insight 2: Model Suitability in High-Detail 3D Reconstructions: The significant disparity in the performance of TensoRF compared to the other two models, particularly in precision and recall, indicates that not all NeRF models are equally suited for tasks requiring high-detail 3D reconstructions. This highlights the importance of model selection based on the specific requirements of the application.

Insight 3: Divergence in 2D Image Quality and 3D Reconstruction in Instant-NGP:. A detailed examination reveals that Instant-NGP demonstrates notable strength in 2D image quality metrics such as PSNR, SSIM, and LPIPS, reflecting its ability to produce superior rendered image quality. However, this excellence in 2D imaging does not correspondingly extend to 3D reconstruction metrics like
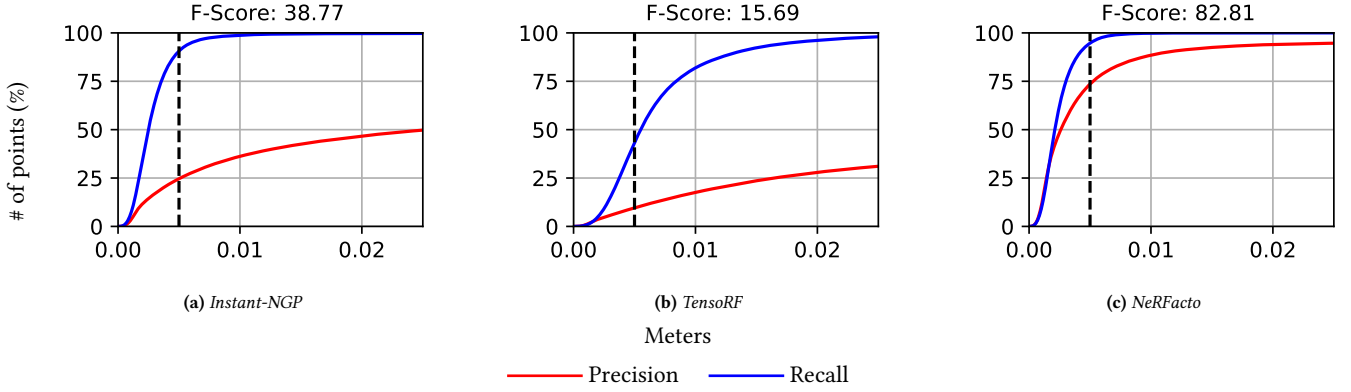
Fig. 11. *Precision-Recall Curves (Scenario-I) based on varying distance threshold after 30,000 iterations*

Precision, Recall, and F1 Score. This observation highlights a significant distinction in the challenges associated with optimizing for high-quality image rendering as opposed to achieving accurate 3D representations. The model's adeptness at rendering highly detailed 2D images does not necessarily imply its effectiveness in accurately reconstructing complex 3D structures, particularly in the context of intricate plant models. This insight underscores the need for a nuanced approach in evaluating the performance of models that are tasked with both 2D image rendering and 3D spatial reconstruction.

3.2 Scenario II - Multiple Plants Indoors

The estimated camera poses from colmap are visualized in Fig. 12. We observe marked differences in model behaviors compared to the single plant scenario, which are likely attributed to the added intricacy of multiple plants in a single scene. Results are illustrated in the Fig. 13.

Precision: Instant-NGP shows a steady increase in precision with more iterations, starting from 0.57 at 100 iterations and peaking at 23.45 at 30000 iterations. However, NeRFacto starts at a higher precision of 7.77 at 100 iterations and reaches a higher peak of 64.47 at 30000 iterations, indicating a more accurate reconstruction of the corn plants. TensoRF, although it improves with more iterations, lags behind the others, starting at 1.51 and reaching 20.50 at 30000 iterations. It is further illustrated in Fig. 14.

Recall: For recall, a similar pattern is observed. Instant-NGP's recall increases from 1.23 to 58.57, NeRFacto from 27.44 to 76.80, and TensoRF from 12.62 to 55.34 across iterations. NeRFacto consistently maintains a higher recall, suggesting its superior ability to encompass points in the ground truth.. It is further illustrated in Fig. 15.

F1 Score: The F1 Score, balancing precision and recall, also follows this trend. Instant-NGP's F1 score peaks at 33.49, NeRFacto at 70.10, and TensoRF at 29.91, all at 30000 iterations. NeRFacto demonstrates the best balance between precision and recall.

PSNR:. In terms of PSNR, which evaluates the quality of rendered images, all models show improvement with more iterations. Instant-NGP goes from 13.70 to 19.08, NeRFacto from 14.93 to 18.93, and

TensoRF from 13.38 to 15.54. Instant-NGP achieves the highest PSNR, suggesting better image quality.

SSIM:. For SSIM, higher values indicate better image structure similarity. Instant-NGP progresses from 0.36 to 0.64, NeRFacto from 0.35 to 0.64, and TensoRF from 0.35 to 0.42. Both Instant-NGP and NeRFacto perform similarly and better than TensoRF in this aspect.

LPIPS:. Lower LPIPS values signify higher perceptual similarity to the ground truth. Instant-NGP decreases from 0.89 to 0.31, NeRFacto from 0.77 to 0.25, and TensoRF from 0.83 to 0.56, with NeRFacto showing the best perceptual image quality.

Computation Time: The time taken for iterations is crucial for efficiency. Instant-NGP and NeRFacto have comparable times, but TensoRF takes significantly longer at higher iterations, indicating less time efficiency.

Overall Performance and Suitability: NeRFacto emerges as the most balanced and efficient model, exhibiting high precision, recall, and F1 scores, along with favorable PSNR, SSIM, and LPIPS values. Its efficiency in time taken is also comparable to Instant-NGP. Instant-NGP, while showing improvements, doesn't quite match NeRFacto's balance of precision and recall. TensoRF, despite its merits, falls behind in several key metrics, particularly in precision, recall, SSIM, and LPIPS. Detailed results are given in Table 4, after complete training. For more granular look, consult the supplementary Table 7. The Precision-Recall Curves based on varying distance threshold after maximum training of 30,000 iterations is given in Fig. 16.

Insight 1: Improved Performance of TensoRF in Scenario 2: In the second scenario, TensoRF demonstrated a notable improvement compared to its performance in the first scenario. Specifically, its F1 score, a critical metric for 3D modeling accuracy, significantly increased from 15.69 in the first scenario to 29.91 after 30,000 iterations in the second scenario. This substantial improvement highlights TensoRF's potential in more complex or demanding 3D modeling tasks, especially when allowed to complete its training process.

Insight 2: 2D Metrics Versus 3D F1 Score for Instant-NGP and NeRFacto: While Instant-NGP and NeRFacto show comparable results in 2D image quality metrics such as PSNR and SSIM, a distinct difference
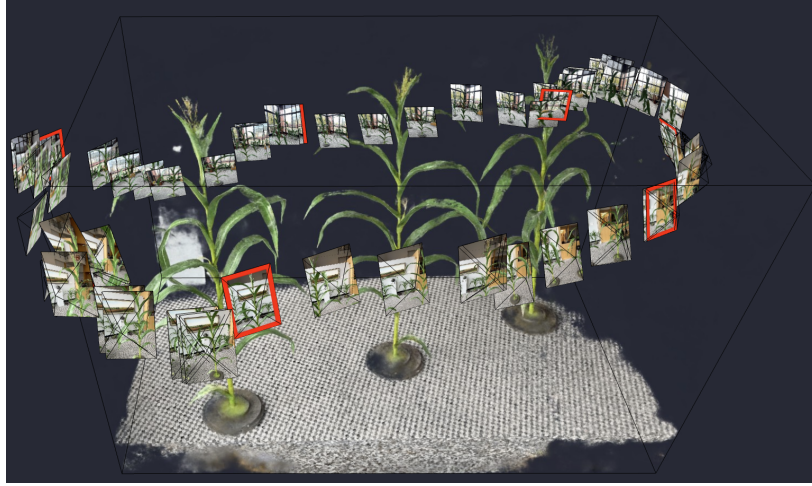
Fig. 12. *Camera Pose Estimations for Scenario-II*

(a) *PSNR*

(b) *SSIM*

(c) *LPIPS*

(d) *Precision*

(e) *Recall*

(f) *F1 Score*

Number of Iterations

Instant-NGP ——— NeRFacto ——— TensoRF
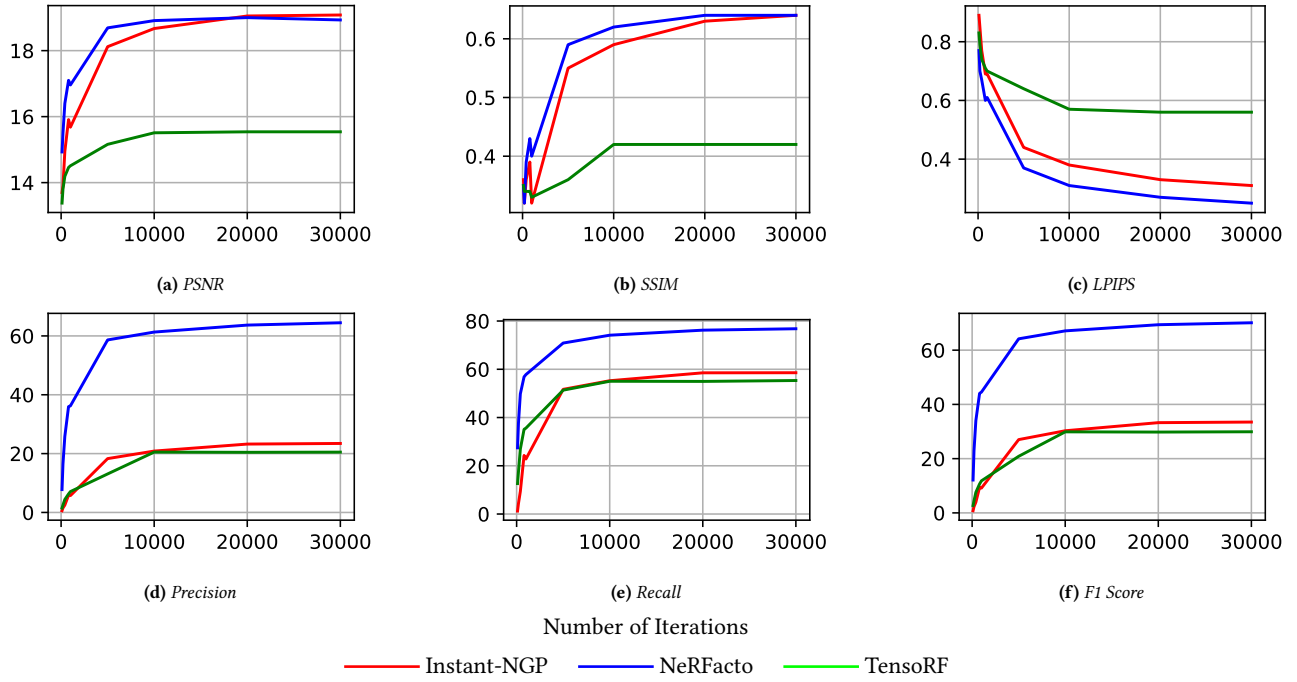
Fig. 13. *Combined Comparison of 2D Image Quality (top) and 3D Geometry (bottom) Metrics for Scenario-II*

Table 4. *Performance metrics of NeRFs reconstruction techniques - Scenario II*

Model Name	Precision ↑	Recall ↑	F1 ↑	PSNR ↑	SSIM ↑	LPIPS ↓	Time(s) ↓
Instant-NGP	23.45	58.57	33.49	19.08	0.64	0.31	1886
NeRFacto	64.47	76.8	70.1	18.93	0.64	0.25	1226
TensoRF	20.5	55.34	29.91	15.54	0.42	0.56	2607

is observed in their 3D modeling capabilities, as reflected in their F1 scores, as observed in last scenario. This suggests that NeRFacto might be a more reliable choice for applications requiring high accuracy in 3D reconstructions.

(a) *Instant-NGP*

(b) *TensoRF*

(c) *NeRFacto*

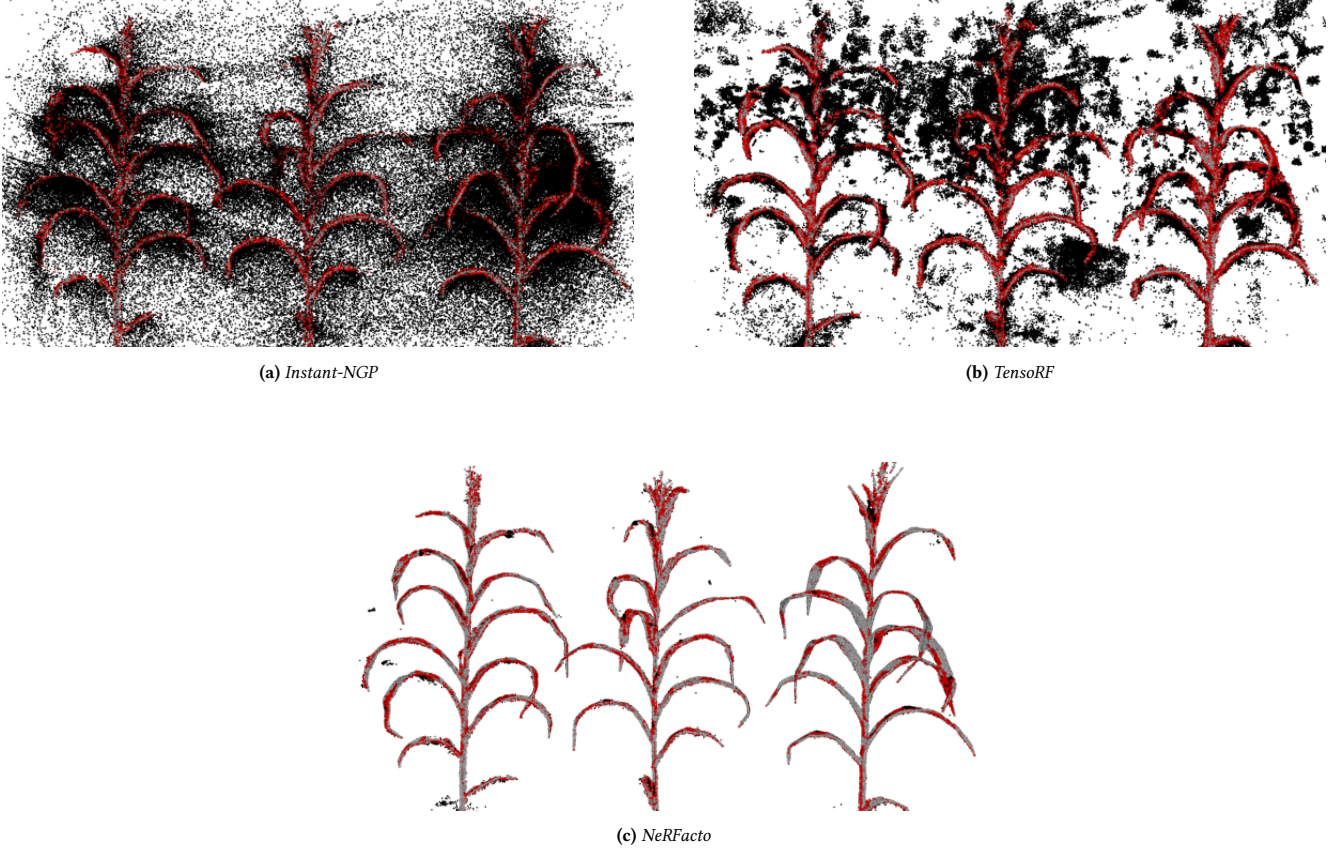**Fig. 14.** *Precision of 3D reconstruction of NeRF techniques - Scenario II*

3.3 Scenario III - Multiple Plants Outdoors

The estimated camera poses from colmap are visualized in Fig. 17

The results from our evaluation of three state-of-the-art NeRF techniques for 3D plant structure reconstruction are illustrated in the Fig. 18. Please note that the value of threshold distance d for 3d metrics was considered 0.01, as compared to 0.005 in last two scenarios.

Precision: Across all iterations, NeRFacto consistently demonstrates the highest precision, peaking at 68.29% at 60000 iterations, suggesting its superior ability to reconstruct points close to the ground truth. Instant-NGP shows a steady increase in precision with more iterations, yet never surpasses NeRFacto, reaching a maximum of 15.06%. TensoRF, while starting lower, reaches a comparable precision to Instant-NGP at higher iterations (40.95% at 60000 iterations). It is further illustrated in Fig. 19.

Recall: NeRFacto also leads in recall, achieving a high of 82.32% at 60000 iterations, indicating its effectiveness in encompassing points from the ground truth. Instant-NGP shows significant improvement with increased iterations, reaching a recall of 59.55%, but remains behind NeRFacto. TensoRF shows substantial growth in recall, ultimately achieving 75.62%, positioning it between Instant-NGP and NeRFacto in terms of completeness. It is further illustrated in Fig. 20.

F1 Score: Reflecting the balance between precision and recall, the F1 scores show NeRFacto as the superior model, with a peak score of 74.65% at 60000 iterations. Instant-NGP's F1 score also improves with more iterations but tops out at 24.04%, significantly lower than NeRFacto. TensoRF's F1 score, while lower than NeRFacto's, surpasses Instant-NGP, reaching 53.13% at 60000 iterations.

PSNR:. In terms of image quality, as measured by PSNR, all models show incremental improvements with more iterations. Instant-NGP and NeRFacto display similar trends, with NeRFacto slightly leading, peaking at 16.70 at 60000 iterations. TensoRF shows a comparable maximum PSNR of 17.32, suggesting its slight edge in rendering higher-quality images.

SSIM:. For the SSIM metric, all three models show improvements with increased iterations. NeRFacto maintains a slight advantage over the others, peaking at 0.32 at 60000 iterations, indicating its better performance in maintaining structural integrity in the rendered images. Instant-NGP and TensoRF show similar SSIM scores, with TensoRF slightly leading at higher iterations.

LPIPS:. The LPIPS scores, which assess perceptual similarity, decrease for all models with more iterations, indicating improved performance. NeRFacto and TensoRF show similar trends, with NeRFacto having a slight edge, achieving a score of 0.34 at 60000
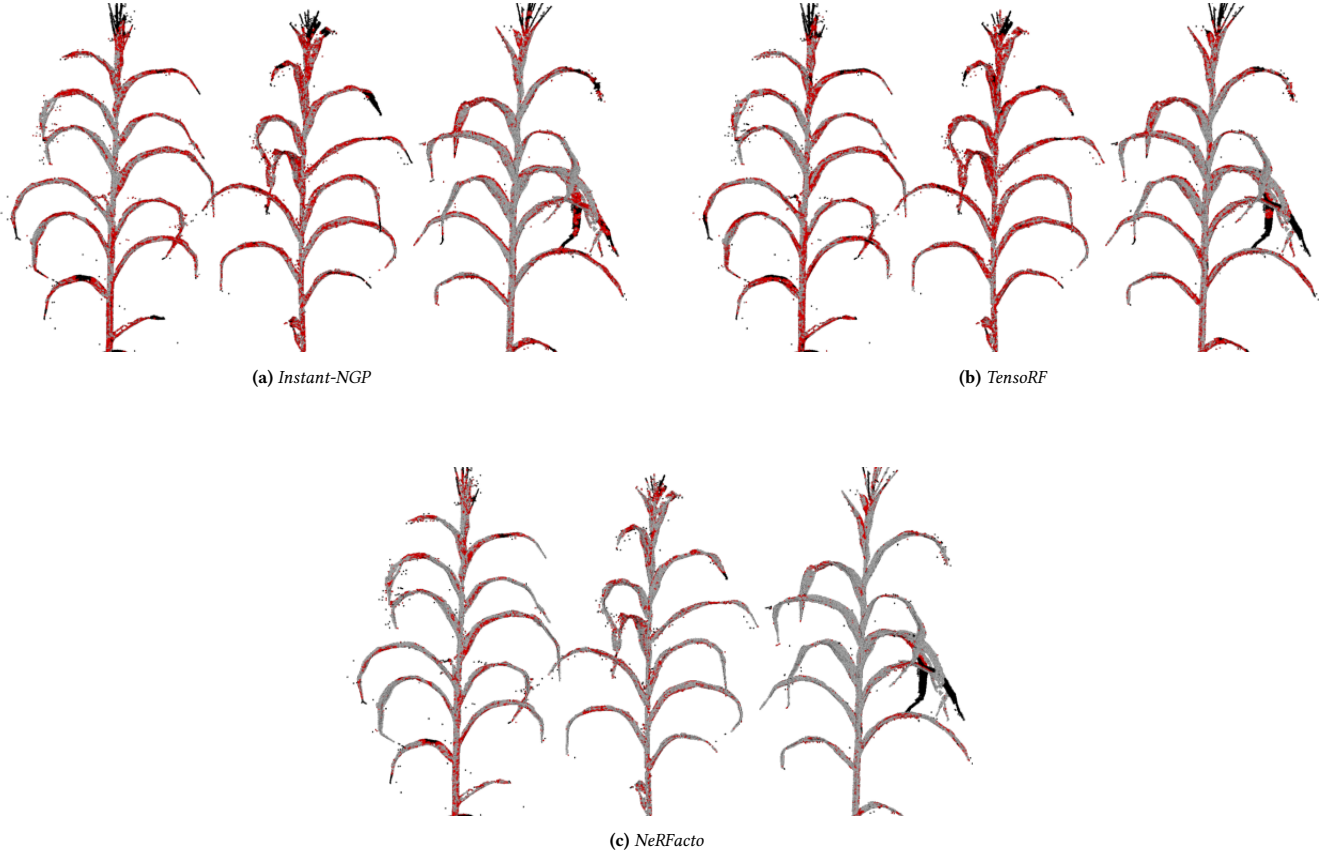
(a) *Instant-NGP*

(b) *TensoRF*

(c) *NeRFacto*

Fig. 15. *Recall of 3D reconstruction of NeRF techniques - Scenario II*

(a) *Instant-NGP*

(b) *TensoRF*

(c) *NeRFacto*

Meters
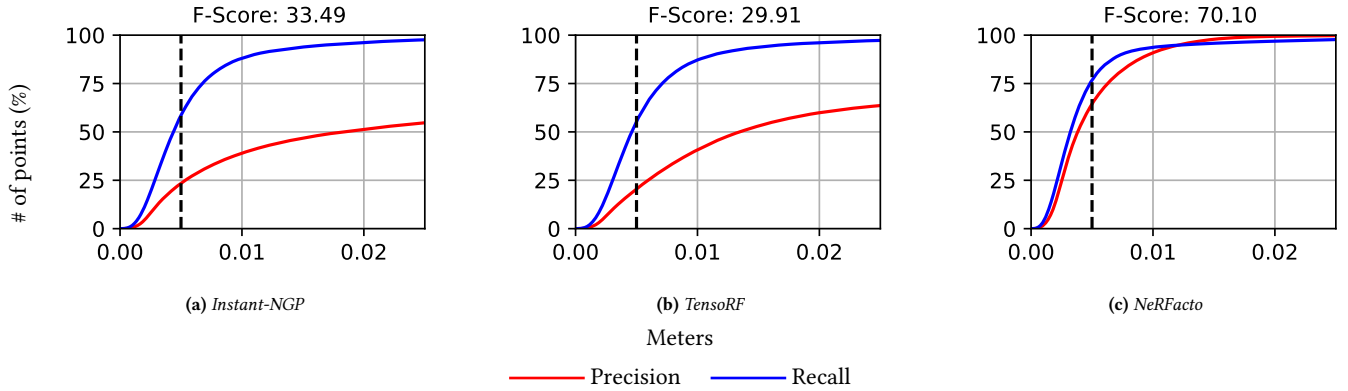
—— Precision —— Recall

Fig. 16. *Precision-Recall Curves (Scenario-II) based on varying distance threshold after 30,000 iterations*

iterations compared to TensoRF's 0.55. Instant-NGP's performance is consistently lower in this metric.

Computation Time: In terms of efficiency, Instant-NGP and NeRFacto are the fastest, followed by TensoRF.

Overall Performance and Suitability: NeRFacto again emerges as the most balanced and robust model, excelling in precision, recall, F1 score, and LPIPS. Detailed results are given in Table 5, after complete

training. For more granular look, consult the supplementary Table 8. The Precision-Recall Curves based on varying distance threshold after maximum training of 60,000 iterations is given in Fig. 21.

Insight 1: Enhanced Performance of TensoRF in Outdoor Settings: TensoRF demonstrates significant improvement in its performance in the third scenario compared to the first. Specifically, its F1 score has seen a notable increase; from 15.69 in the first scenario to 29.91

Fig. 17. *Camera Pose Estimations for Scenario-III*

(a) *PSNR*   **(b)** *SSIM*   **(c)** *LPIPS*

(d) *Precision*   **(e)** *Recall*   **(f)** *F1 Score*

Number of Iterations

Instant-NGP   NeRFacto   TensoRF
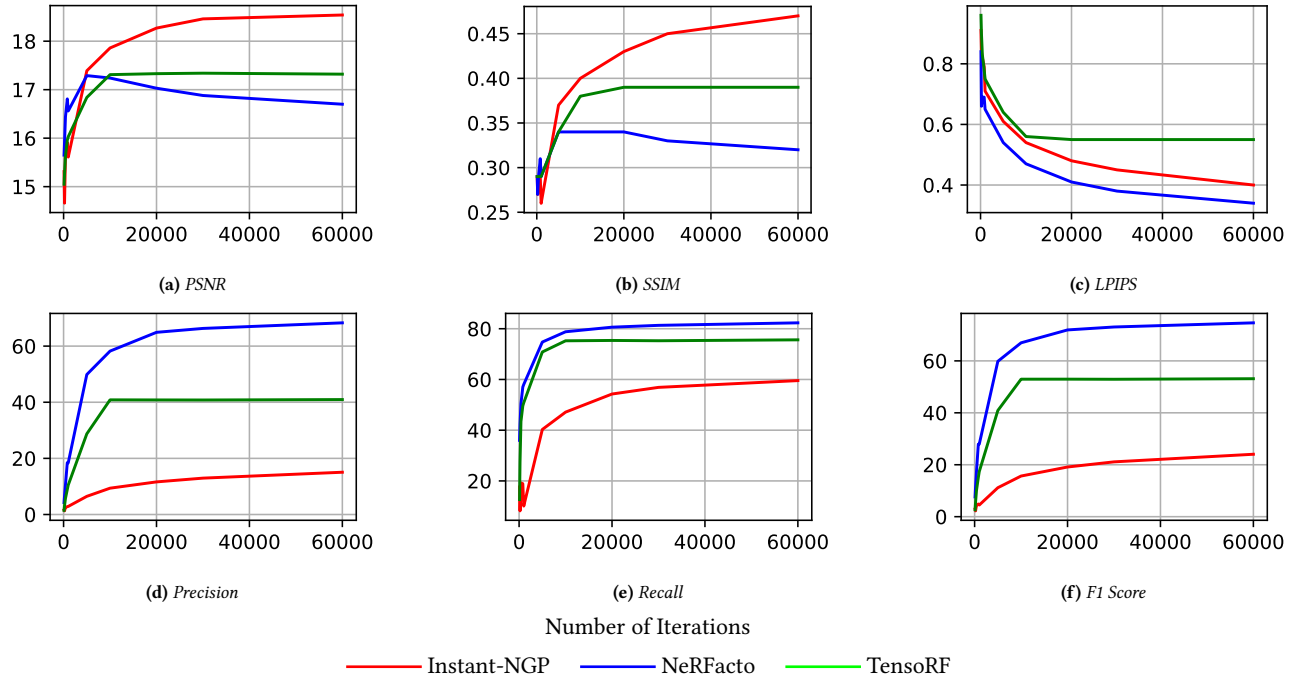
Fig. 18. *Combined Comparison of 2D Image Quality (top) and 3D Geometry (bottom) Metrics for Scenario-III*

Table 5. *Performance metrics of NeRFs reconstruction techniques - Scenario III*

Model Name	Precision ↑	Recall ↑	F1 ↑	PSNR ↑	SSIM ↑	LPIPS ↓	Time(s) ↓
Instant-NGP	15.06	59.55	24.04	18.54	0.47	0.4	1466
NeRFacto	68.29	82.32	74.65	16.7	0.32	0.34	1499
TensoRF	40.95	75.62	53.13	17.32	0.39	0.55	1965

in the second, and reaching 53.13 after 30,000 iterations in the current outdoor scenario. This upward trajectory in F1 scores, which is a balanced measure of precision and recall, indicates TensoRF's

enhanced capability in outdoor environments, potentially outperforming Instant-NGP in these settings. This suggests that TensoRF might be a more suitable choice for outdoor 3D modeling tasks
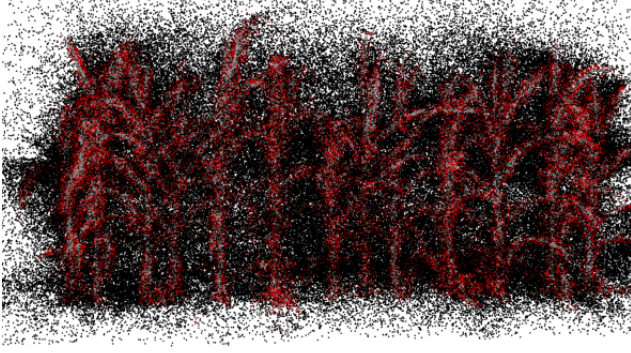
(a) *Instant-NGP*

(b) *TensoRF*
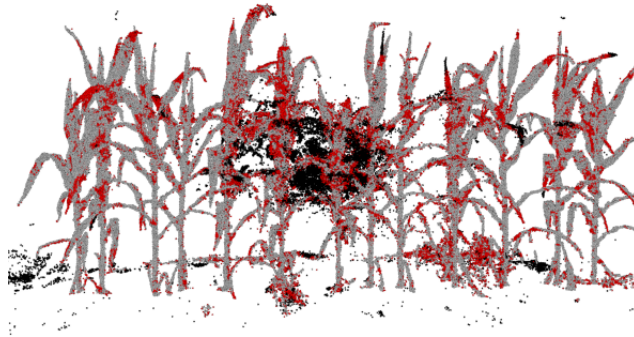
(c) *NeRFacto*

Fig. 19. *Precision of 3D reconstruction of NeRF techniques - Scenario II*

where both precision and completeness are crucial. This property may have contributed in the selection of TensoRF as a building block for using multiple local radiance fields, during in-the-wild reconstruction, in the recent paper [41].

Insight 2: LPIPS as a Strong Indicator of 3D Model Quality: The LPIPS metric appears to be a more representative measure of the quality of the resulting 3D models. In the analysis, we observe that models with lower LPIPS scores consistently show better performance across other metrics. This trend indicates the relevance of LPIPS in assessing the perceptual quality of 3D models. The further investigation into how LPIPS correlates with other metrics could provide deeper insights into model performance, especially in the context of realistic and perceptually accurate 3D reconstructions.

4 DISCUSSION

The difference in the output quality between Instant-NGP and Nerfacto, especially concerning the density and crispness of the rendered scenes, could indeed be related to the sampling strategies used by each algorithm.

Instant-NGP Sampling Strategy: Instant-NGP uses an improved training and rendering algorithm that involves a ray marching scheme with an occupancy grid. This means that when the algorithm shoots

rays into the scene to sample colors and densities, it uses an occupancy grid to skip over empty space, as well as areas behind high-density regions to improve efficiency.

- The occupancy grid used in Instant-NGP is a multiscale grid that coarsely marks empty and non-empty space and is used to determine where to skip samples to speed up processing.

- This approach is quite effective in terms of speed, leading to significant improvements over naive sampling methods.

- However, if the occupancy grid isn't fine-grained enough or if the method for updating this grid isn't capturing the scene's density variations accurately, it could lead to a "muddy" or overly dense rendering because it might not be sampling the necessary areas with enough precision.

Nerfacto Sampling Strategy: Nerfacto, on the other hand, uses a combination of different sampling techniques:

- *Camera Pose Refinement:* By refining camera poses, Nerfacto ensures that the samples taken are based on more accurate viewpoints, which directly affects the clarity of the rendered images.

- *Piecewise Sampler:* This sampler is used to produce an initial set of samples, with a distribution that allows both dense

(a) *Instant-NGP*

(b) *TensoRF*

(c) *NeRFacto*

Fig. 20. *Recall of 3D reconstruction of NeRF techniques - Scenario II*

(a) *Instant-NGP*

(b) *TensoRF*

(c) *NeRFacto*
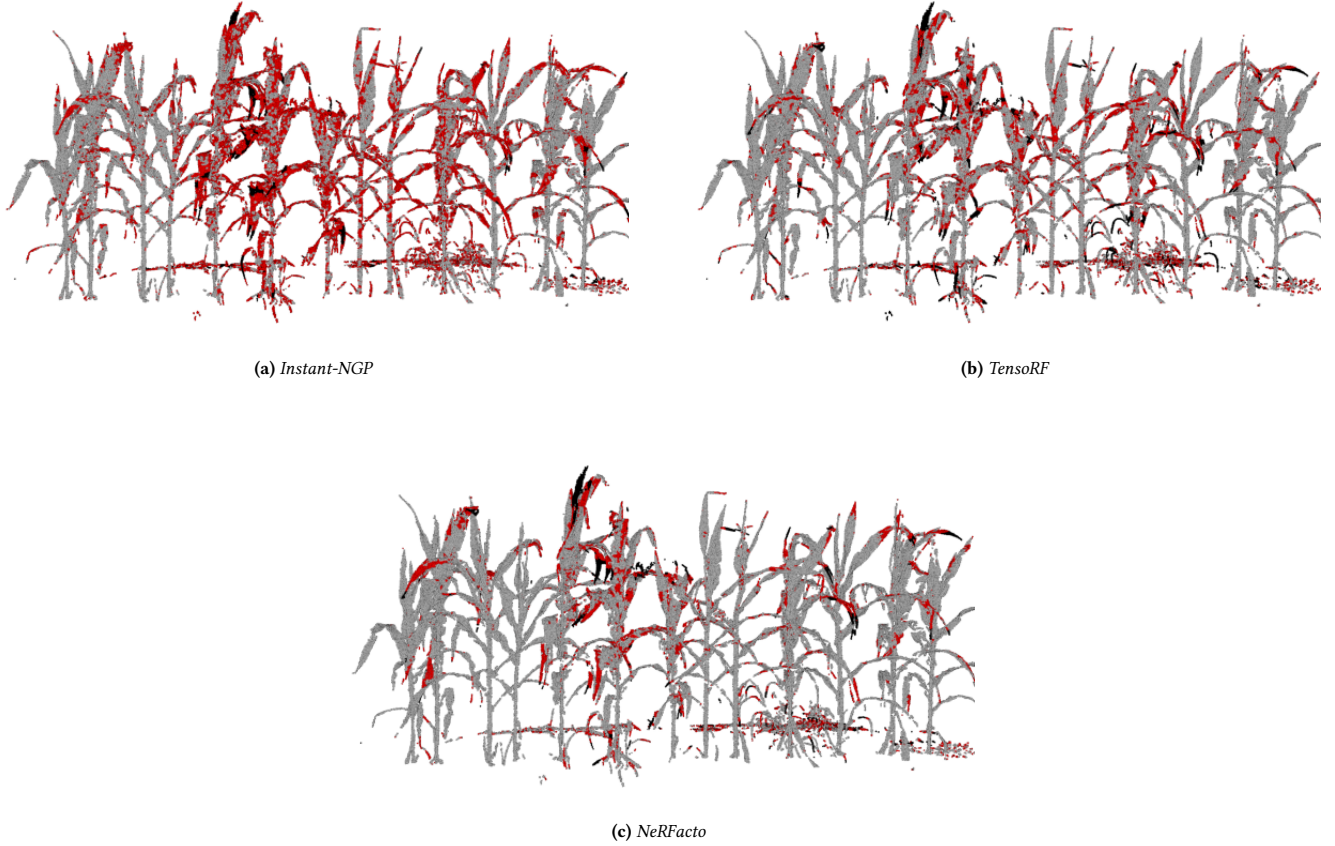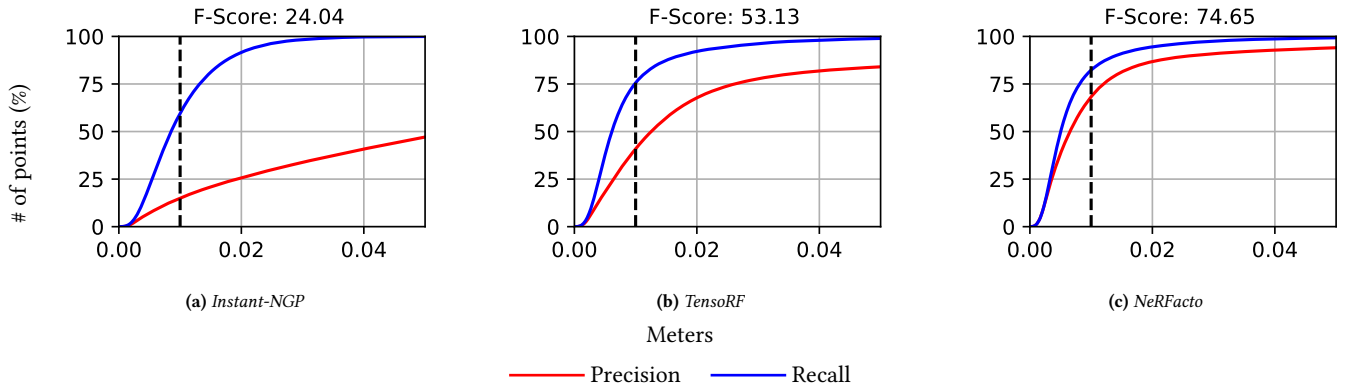
Fig. 21. *Precision-Recall Curves (Scenario-III) based on varying distance threshold after 60,000 iterations*

sampling near the camera and appropriate sampling further away. This could lead to clearer images since it captures details both near and far from the camera.

- *Proposal Sampler:* This is a key part of the Nerfacto method. It uses a proposal network to concentrate sample locations in regions that contribute most to the final render, usually around the first surface intersection. This targeted sampling

could be a major reason why Nerfacto produces crisper images—it focuses computational resources on the most visually significant parts of the scene.

- *Density Field:* By using a density field guided by a hash encoding and a small fused MLP, Nerfacto can efficiently guide sampling even further. It doesn't require an extremely detailed density map since it is used primarily for guiding

the sampling process, which means that it balances quality and speed without necessarily impacting the final image's detail.

Comparing Sampling Strategies: Instant-NGP's sampling strategy is built for speed, with an occupancy grid that helps skip irrelevant samples. This approach is great for real-time applications but can potentially miss subtle density variations, leading to a denser and less clear output if the grid isn't capturing all the necessary detail. Nerfacto's sampling strategy is more complex and layered, with multiple mechanisms in place to ensure that sampling is done more effectively in areas that greatly affect the visual output. The combination of pose refinement, piecewise sampling, proposal sampling, and an efficient density field leads to more accurate sampling, which in turn produces crisper images. In summary, the reason for Nerfacto's superior crispness likely stems from its more refined and targeted approach to sampling, which concentrates computational efforts on the most visually impactful parts of the scene. In contrast, Instant-NGP's faster but less targeted sampling may result in less clarity and more visual artifacts.

5 CONCLUSIONS

The findings of this research are important for precision agriculture, offering a non-destructive and efficient method for detailed plant analysis. The ability to accurately reconstruct plant structures in 3D without physically altering or harming the plant is a key advancement. This non-intrusive approach enables essential agricultural tasks such as growth monitoring, yield prediction, and early disease detection to be performed more effectively, without the need for physical sampling or destruction of the plants. Furthermore, this research extends its impact beyond immediate applications.

In addition to these methodological advancements, our study contributes valuable resources for ongoing research. We collected a comprehensive dataset comprising images and ground truth 3D LiDAR scans, which will be instrumental for further studies. This dataset not only facilitates the testing and validation of current models but also serves as a benchmark for the development and evaluation of future NeRF models in agricultural contexts. Moreover, we developed a robust framework for the evaluation of NeRF models, which can be adapted and utilized in future research. This framework is designed to assess various aspects of model performance, ensuring a comprehensive evaluation of new techniques as they emerge. Moreover, this groundwork sets the stage for our next focus.

Our research also provides detailed insights into the performance of each model, identifying their strengths and limitations in various scenarios. These insights and resources pave the way for future research at the nexus of NeRF technologies and agriculture. The detailed analysis and case studies presented in this paper will be invaluable for researchers and practitioners looking to leverage NeRF in agricultural applications, contributing to the development of more advanced, efficient, and sustainable agricultural practices.

REFERENCES

[1] Luis Santos Pereira. Water, agriculture and food: challenges and issues. *Water Resources Management*, 31(10):2985–2999, 2017.

[2] Pankaj Kumar, Jinhai Cai, and Stan Miklavcic. High-throughput 3d modelling of plants for phenotypic analysis. In *Proceedings of the 27th conference on image and vision computing New Zealand*, pages 301–306, 2012.

[3] Abhipray Paturkar, Gourab Sen Gupta, and Donald Bailey. Making use of 3d models for plant physiognomic analysis: A review. *Remote Sensing*, 13(11):2232, 2021.

[4] Ben Mildenhall, Pratul P Srinivasan, Matthew Tancik, Jonathan T Barron, Ravi Ramamoorthi, and Ren Ng. NeRF: Representing scenes as neural radiance fields for view synthesis. *Communications of the ACM*, 65(1):99–106, 2021.

[5] Anette Eltner and Giulia Sofia. Structure from motion photogrammetric technique. In *Developments in Earth surface processes*, volume 23, pages 1–24. Elsevier, 2020.

[6] Rui Chen, Songfang Han, Jing Xu, and Hao Su. Point-based multi-view stereo network. In *Proceedings of the IEEE/CVF international conference on computer vision*, pages 1538–1547, 2019.

[7] Nianchen Deng, Zhenyi He, Jiannan Ye, Budmonde Duinkharjav, Praneeth Chakravarthula, Xubo Yang, and Qi Sun. Fov-NeRF: Foveated neural radiance fields for virtual reality. *IEEE Transactions on Visualization and Computer Graphics*, 28(11):3854–3864, 2022.

[8] Matthew Tancik, Vincent Casser, Xinchen Yan, Sabeek Pradhan, Ben Mildenhall, Pratul P Srinivasan, Jonathan T Barron, and Henrik Kretzschmar. Block-NeRF: Scalable large scene neural view synthesis. In *Proceedings of the IEEE/CVF Conference on Computer Vision and Pattern Recognition*, pages 8248–8258, 2022.

[9] Shenglian Lu, Chunjiang Zhao, Xinyu Guo, et al. Venation skeleton-based modeling plant leaf wilting. *International Journal of Computer Games Technology*, 2009, 2009.

[10] JB Evers. 3D modelling of branching in plants. In *Proceedings of the MODSIM2011, 19th International Congress on Modelling and Simulation, 12-16 December 2011, Perth, Australia*, pages 982–988, 2011.

[11] Abhipray Paturkar, Gaurab Sen Gupta, and Donald Bailey. 3D reconstruction of plants under outdoor conditions using image-based computer vision. In *Recent Trends in Image Processing and Pattern Recognition: Second International Conference, RTIP2R 2018, Solapur, India, December 21–22, 2018, Revised Selected Papers, Part III 2*, pages 284–297. Springer, 2019.

[12] Sheng Wu, Weiliang Wen, Yongjian Wang, Jiangchuan Fan, Chuanyu Wang, Wenbo Gou, and Xinyu Guo. MVS-Pheno: a portable and low-cost phenotyping platform for maize shoots using multiview stereo 3d reconstruction. *Plant Phenomics*, 2020.

[13] Yinghua Wang, Songtao Hu, He Ren, Wanneng Yang, and Ruifang Zhai. 3DPhenoMVS: A low-cost 3d tomato phenotyping pipeline using 3d reconstruction point cloud based on multiview images. *Agronomy*, 12(8):1865, 2022.

[14] Dionisio Andújar, Mikel Calle, César Fernández-Quintanilla, Ángela Ribeiro, and José Dorado. Three-dimensional modeling of weed plants using low-cost photogrammetry. *Sensors*, 18(4):1077, 2018.

[15] Guoyu Lu. Bird-view 3d reconstruction for crops with repeated textures. In *2023 IEEE/RSJ International Conference on Intelligent Robots and Systems (IROS)*, pages 4263–4270. IEEE, 2023.

[16] Abhipray Paturkar, Gourab Sen Gupta, and Donald Bailey. Effect on quality of 3d model of plant with change in number and resolution of images used: an investigation. In *Advances in Signal and Data Processing: Select Proceedings of ICSDP 2019*, pages 377–388. Springer, 2021.

[17] Joanna Alina Setkowicz. Evaluation of algorithms and tools for 3d modeling of laser scanning data. Master's thesis, Institutt for bygg, anlegg og transport, 2014.

[18] Jean Liénard, Andre Vogs, Demetrios Gatziolis, and Nikolay Strigul. Embedded, real-time uav control for improved, image-based 3d scene reconstruction. *Measurement*, 81:264–269, 2016.

[19] Xiaoying Tang, Mengjun Wang, Qian Wang, Jingjing Guo, and Jingxiao Zhang. Benefits of terrestrial laser scanning for construction qa/qc: a time and cost analysis. *Journal of Management in Engineering*, 38(2):05022001, 2022.

[20] Thuy Tuong Nguyen, David C Slaughter, Nelson Max, Julin N Maloof, and Neelima Sinha. Structured light-based 3D reconstruction system for plants. *Sensors*, 15(8):18587–18612, 2015.

[21] Adrian Azzarelli, Nantheera Anantrasirichai, and David R Bull. Towards a robust framework for NeRF evaluation. *arXiv preprint arXiv:2305.18079*, 2023.

[22] Lukas Radl, Andreas Kurz, and Markus Steinberger. Analyzing the internals of neural radiance fields. *arXiv preprint arXiv:2306.00696*, 2023.

[23] Sicheng Li, Hao Li, Yue Wang, Yiyi Liao, and Lu Yu. SteerNeRF: Accelerating NeRF rendering via smooth viewpoint trajectory. In *Proceedings of the IEEE/CVF Conference on Computer Vision and Pattern Recognition*, pages 20701–20711, 2023.

[24] Fabio Remondino, Ali Karami, Ziyang Yan, Gabriele Mazzacca, Simone Rigon, and Rongjun Qin. A critical analysis of NeRF-based 3d reconstruction. *Remote Sensing*, 15(14):3585, 2023.

[25] E Balloni, L Gorgoglione, M Paolanti, A Mancini, and R Pierdicca. Few shot photogrametry: A comparison between NeRF and MVS-SfM for the documentation

of cultural heritage. *The International Archives of the Photogrammetry, Remote Sensing and Spatial Information Sciences*, 48:155–162, 2023.

[26] Anushrut Jignasu, Ethan Herron, Talukder Zaki Jubery, James Afful, Aditya Balu, Baskar Ganapathysubramanian, Soumik Sarkar, and Adarsh Krishnamurthy. Plant geometry reconstruction from field data using neural radiance fields. In *2nd AAAI Workshop on AI for Agriculture and Food Systems*, 2023.

[27] Thomas Müller, Alex Evans, Christoph Schied, and Alexander Keller. Instant neural graphics primitives with a multiresolution hash encoding. *ACM Transactions on Graphics (ToG)*, 41(4):1–15, 2022.

[28] Matthew Tancik, Ethan Weber, Evonne Ng, Ruilong Li, Brent Yi, Terrance Wang, Alexander Kristoffersen, Jake Austin, Kamyar Salahi, Abhik Ahuja, et al. NeRF-Studio: A modular framework for neural radiance field development. In *ACM SIGGRAPH 2023 Conference Proceedings*, pages 1–12, 2023.

[29] Anpei Chen, Zexiang Xu, Andreas Geiger, Jingyi Yu, and Hao Su. TensoRF: Tensorial radiance fields. In *European Conference on Computer Vision*, pages 333–350. Springer, 2022.

[30] Jonathan T Barron, Ben Mildenhall, Dor Verbin, Pratul P Srinivasan, and Peter Hedman. Mip-nerf 360: Unbounded anti-aliased neural radiance fields. In *Proceedings of the IEEE/CVF Conference on Computer Vision and Pattern Recognition*, pages 5470–5479, 2022.

[31] Arno Knapitsch, Jaesik Park, Qian-Yi Zhou, and Vladlen Koltun. Tanks and Temples: Benchmarking large-scale scene reconstruction. *ACM Transactions on Graphics (ToG)*, 36(4):1–13, 2017.

[32] Paul J Besl and Neil D McKay. Method for registration of 3-d shapes. In *Sensor fusion IV: control paradigms and data structures*, volume 1611, pages 586–606. Spie, 1992.

[33] Zhengyou Zhang. Iterative point matching for registration of free-form curves and surfaces. *International journal of computer vision*, 13(2):119–152, 1994.

[34] Seth D Billings, Emad M Boctor, and Russell H Taylor. Iterative most-likely point registration (imlp): A robust algorithm for computing optimal shape alignment. *PloS one*, 10(3):e0117688, 2015.

[35] G Mazzacca, A Karami, S Rigon, EM Farella, P Trybala, and F Remondino. NeRF for heritage 3D reconstruction. *The International Archives of the Photogrammetry, Remote Sensing and Spatial Information Sciences*, 48:1051–1058, 2023.

[36] Zhou Wang, Alan C Bovik, Hamid R Sheikh, and Eero P Simoncelli. Image quality assessment: from error visibility to structural similarity. *IEEE transactions on image processing*, 13(4):600–612, 2004.

[37] Alain Hore and Djemel Ziou. Image quality metrics: Psnr vs. ssim. In *2010 20th international conference on pattern recognition*, pages 2366–2369. IEEE, 2010.

[38] Richard Zhang, Phillip Isola, Alexei A Efros, Eli Shechtman, and Oliver Wang. The unreasonable effectiveness of deep features as a perceptual metric. In *Proceedings of the IEEE conference on computer vision and pattern recognition*, pages 586–595, 2018.

[39] Qiangeng Xu, Zexiang Xu, Julien Philip, Sai Bi, Zhixin Shu, Kalyan Sunkavalli, and Ulrich Neumann. Point-NeRF: Point-based neural radiance fields. In *Proceedings of the IEEE/CVF Conference on Computer Vision and Pattern Recognition*, pages 5438–5448, 2022.

[40] Jason Zhang, Gengshan Yang, Shubham Tulsiani, and Deva Ramanan. NeRS: Neural reflectance surfaces for sparse-view 3d reconstruction in the wild. *Advances in Neural Information Processing Systems*, 34:29835–29847, 2021.

[41] Andreas Meuleman, Yu-Lun Liu, Chen Gao, Jia-Bin Huang, Changil Kim, Min H Kim, and Johannes Kopf. Progressively optimized local radiance fields for robust view synthesis. In *Proceedings of the IEEE/CVF Conference on Computer Vision and Pattern Recognition*, pages 16539–16548, 2023.

SUPPLEMENT

Table 6. *Performance metrics of NeRFs reconstruction techniques - Scenario I*

Model Name	Iterations	Precision ↑	Recall ↑	F1 ↑	PSNR ↑	SSIM ↑	LPIPS ↓	Time(s) ↓
Instant-NGP	100	0.29	2.48	0.53	17.14	0.58	0.81	13
Instant-NGP	200	0.32	1.50	0.53	18.23	0.56	0.75	26
Instant-NGP	400	1.25	7.14	2.13	19.64	0.60	0.66	42
Instant-NGP	800	5.66	35.17	9.74	21.21	0.64	0.55	61
Instant-NGP	1000	3.93	27.61	6.88	20.71	0.57	0.59	76
Instant-NGP	5000	21.93	89.03	35.20	22.73	0.76	0.28	175
Instant-NGP	10000	25.98	92.59	40.57	23.20	0.79	0.22	297
Instant-NGP	20000	23.21	88.38	36.77	23.42	0.81	0.18	527
Instant-NGP	30000	24.66	90.62	38.77	23.41	0.81	0.17	756
NeRFacto	100	1.94	20.98	3.55	18.11	0.59	0.75	14
NeRFacto	200	7.72	42.84	13.08	19.50	0.57	0.65	27
NeRFacto	400	20.86	68.64	32.00	21.27	0.64	0.55	43
NeRFacto	800	39.48	80.26	52.92	22.33	0.67	0.45	64
NeRFacto	1000	41.35	82.54	55.09	22.20	0.66	0.44	79
NeRFacto	5000	66.43	92.51	77.33	22.30	0.73	0.19	430
NeRFacto	10000	70.04	93.94	80.25	22.34	0.74	0.15	564
NeRFacto	20000	73.32	94.51	82.58	22.35	0.74	0.13	1068
NeRFacto	30000	73.57	94.72	82.81	22.24	0.73	0.12	1938
TensoRF	100	0.43	2.27	0.72	13.44	0.54	0.82	13
TensoRF	200	0.65	4.47	1.13	13.55	0.52	0.82	25
TensoRF	400	1.18	8.76	2.07	13.51	0.51	0.81	40
TensoRF	800	1.86	14.22	3.29	13.10	0.50	0.79	61
TensoRF	1000	2.05	16.40	3.65	13.14	0.49	0.79	77
TensoRF	5000	6.63	36.57	11.22	13.59	0.52	0.70	420
TensoRF	10000	9.58	43.47	15.69	14.64	0.55	0.67	859
TensoRF	20000	9.51	43.19	15.59	14.68	0.55	0.67	1651
TensoRF	30000	9.58	43.34	15.69	14.69	0.55	0.66	1973

(a) *200 Iterations*   **(b)** *400 Iterations*   **(c)** *800 Iterations*

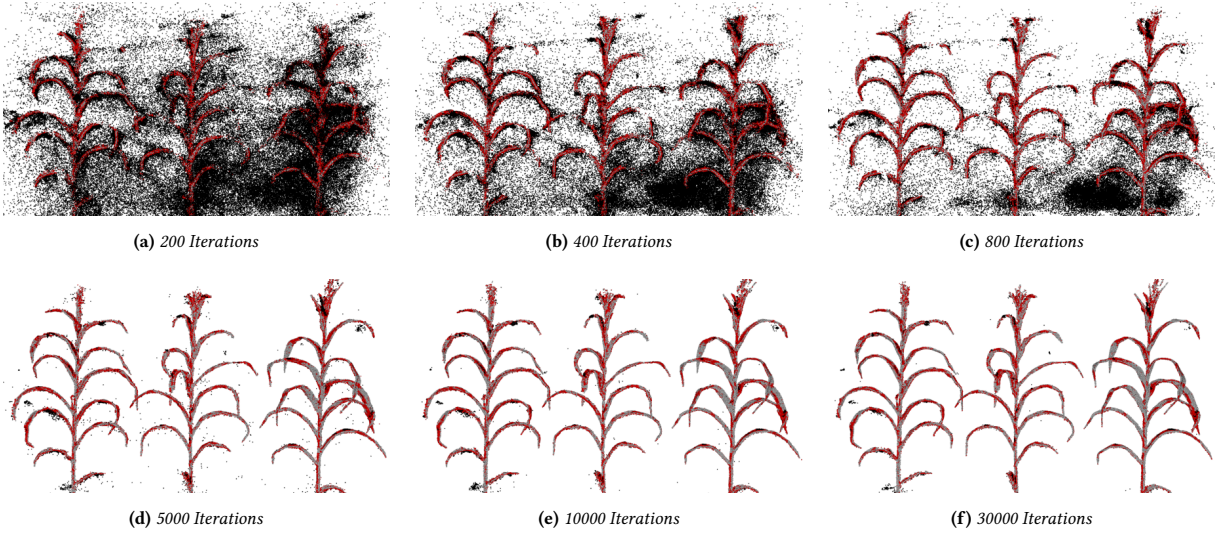**(d)** *5000 Iterations*   **(e)** *10000 Iterations*   **(f)** *30000 Iterations*

Fig. 22. *Precision Over Training Iterations for NeRFacto - Scenario II*

Table 7. *Performance metrics of NeRFs reconstruction techniques - Scenario II*

Model Name	Iterations	Precision ↑	Recall ↑	F1 ↑	PSNR ↑	SSIM ↑	LPIPS ↓	Time(s) ↓
Instant-NGP	100	0.57	1.23	0.78	13.70	0.36	0.89	13
Instant-NGP	200	1.52	4.41	2.27	13.91	0.32	0.85	27
Instant-NGP	400	2.49	9.35	3.93	14.95	0.36	0.77	43
Instant-NGP	800	5.83	24.29	9.41	15.91	0.39	0.69	63
Instant-NGP	1000	5.72	22.80	9.14	15.68	0.32	0.69	78
Instant-NGP	5000	18.30	51.68	27.02	18.12	0.55	0.44	176
Instant-NGP	10000	20.86	55.25	30.28	18.67	0.59	0.38	296
Instant-NGP	20000	23.24	58.53	33.27	19.05	0.63	0.33	1023
Instant-NGP	30000	23.45	58.57	33.49	19.08	0.64	0.31	1886
NeRFacto	100	7.77	27.44	12.12	14.93	0.35	0.77	15
NeRFacto	200	16.42	37.77	22.89	15.51	0.32	0.70	28
NeRFacto	400	25.83	49.81	34.02	16.40	0.39	0.67	44
NeRFacto	800	35.97	56.86	44.07	17.10	0.43	0.60	64
NeRFacto	1000	36.22	57.80	44.53	16.96	0.40	0.61	79
NeRFacto	5000	58.64	70.87	64.18	18.69	0.59	0.37	404
NeRFacto	10000	61.31	74.12	67.11	18.91	0.62	0.31	749
NeRFacto	20000	63.68	76.21	69.38	19.00	0.64	0.27	988
NeRFacto	30000	64.47	76.80	70.10	18.93	0.64	0.25	1226
TensoRF	100	1.51	12.62	2.70	13.38	0.35	0.83	14
TensoRF	200	2.53	17.53	4.43	13.81	0.34	0.79	27
TensoRF	400	4.41	26.94	7.58	14.19	0.34	0.74	44
TensoRF	800	6.28	35.10	10.66	14.46	0.34	0.71	66
TensoRF	1000	7.09	35.61	11.82	14.51	0.33	0.70	82
TensoRF	5000	13.09	51.34	20.86	15.16	0.36	0.64	399
TensoRF	10000	20.51	55.03	29.88	15.51	0.42	0.57	840
TensoRF	20000	20.44	54.97	29.80	15.54	0.42	0.56	1709
TensoRF	30000	20.50	55.34	29.91	15.54	0.42	0.56	2607

Table 8. *Performance metrics of NeRFs reconstruction techniques - Scenario III*

Model Name	Iterations	Precision ↑	Recall ↑	F1 ↑	PSNR ↑	SSIM ↑	LPIPS ↓	Time(s) ↓
Instant-NGP	100	1.61	17.61	2.95	15.31	0.29	0.91	16
Instant-NGP	200	1.29	8.19	2.23	14.66	0.27	0.84	30
Instant-NGP	400	2.45	19.22	4.34	15.65	0.29	0.82	46
Instant-NGP	800	2.81	18.90	4.89	15.91	0.29	0.79	67
Instant-NGP	1000	2.88	10.08	4.48	15.61	0.26	0.71	82
Instant-NGP	5000	6.47	40.28	11.15	17.39	0.37	0.61	186
Instant-NGP	10000	9.38	47.12	15.65	17.86	0.40	0.54	311
Instant-NGP	20000	11.62	54.26	19.13	18.27	0.43	0.48	548
Instant-NGP	30000	12.96	56.88	21.11	18.46	0.45	0.45	783
Instant-NGP	60000	15.06	59.55	24.04	18.54	0.47	0.40	1466
NeRFacto	100	4.26	35.99	7.61	15.65	0.29	0.84	13
NeRFacto	200	6.53	42.49	11.31	15.91	0.27	0.66	27
NeRFacto	400	10.48	50.45	17.35	16.44	0.29	0.69	43
NeRFacto	800	18.49	57.01	27.93	16.81	0.31	0.69	64
NeRFacto	1000	18.39	58.02	27.93	16.56	0.29	0.65	80
NeRFacto	5000	49.87	74.75	59.83	17.29	0.34	0.54	189
NeRFacto	10000	58.22	78.80	66.96	17.24	0.34	0.47	318
NeRFacto	20000	64.91	80.61	71.92	17.03	0.34	0.41	561
NeRFacto	30000	66.30	81.33	73.05	16.88	0.33	0.38	803
NeRFacto	60000	68.29	82.32	74.65	16.70	0.32	0.34	1499
TensoRF	100	1.48	12.65	2.65	15.05	0.29	0.96	17
TensoRF	200	3.05	27.40	5.48	15.26	0.29	0.90	31
TensoRF	400	5.69	43.45	10.06	15.63	0.29	0.83	47
TensoRF	800	8.92	49.59	15.13	15.96	0.29	0.78	68
TensoRF	1000	10.48	50.82	17.37	16.03	0.29	0.75	84
TensoRF	5000	28.74	70.83	40.89	16.84	0.34	0.64	208
TensoRF	10000	40.85	75.24	52.95	17.31	0.38	0.56	374
TensoRF	20000	40.82	75.38	52.96	17.33	0.39	0.55	697
TensoRF	30000	40.80	75.26	52.92	17.34	0.39	0.55	1018
TensoRF	60000	40.95	75.62	53.13	17.32	0.39	0.55	1965

Table 9. *Performance metrics of MipNeRF (failed) reconstruction - Scenario II*

Iterations	Precision ↑	Recall ↑	F1 ↑	PSNR ↑	SSIM ↑	LPIPS ↓	Time (s) ↓
100	0.47	7.57	0.89	11.01	0.34	0.91	26
200	0.63	10.67	1.19	11.24	0.34	0.93	52
400	0.69	12.1	1.3	11.07	0.34	0.92	86
800	0.48	7.68	0.91	9.88	0.33	0.94	158
1000	0.44	7.19	0.82	9.65	0.32	0.94	192
5000	0.35	5.41	0.66	9.31	0.31	0.94	687
10000	0.42	6.29	0.79	8.88	0.29	0.9	1303
20000	0.34	5.3	0.65	8.78	0.28	0.89	2508
30000	0.35	5.71	0.67	9	0.27	0.88	3856